Influence of Low-Temperature Nucleation on the Crystallization Process of Poly(L-lactide)

F. Hernández Sánchez,[†] J. Molina Mateo,[‡] F. J. Romero Colomer,[‡] M. Salmerón Sánchez,[‡] J. L. Gómez Ribelles,[*,‡] and J. F. Mano[§,||]

Centro de Investigaciones Científicas del Yucatán, C.43 No. 130 Chuburná de Hidalgo, CP 97200 Mérida, Mexico, Center for Biomaterials, Universidad Politécnica de Valencia, Camino de Vera s/n, 46022 Valencia, Spain, Polymer Engineering Department, University of Minho, Campus of Azurém, 4800-058 Guimarães, Portugal, and 3B's Research Group—Biomaterials, Biodegradables and Biomimetics, University of Minho, 4710-057 Braga, Portugal

Received May 10, 2005; Revised Manuscript Received July 19, 2005

The crystallization kinetics of poly(L-lactide), PLLA, is slow enough to allow a quasi-amorphous polymer to be obtained at low temperature simply by quenching from the melt. The PLLA crystallization process was followed by differential scanning calorimetry and optical microscopy after nucleation isothermal treatments at temperatures just below (53 °C) and just above (73 °C) the glass transition temperature. The crystallization exotherm shown in the heating thermograms shifts toward lower temperatures as the annealing time at 73 °C increases. The same effect is shown to a lesser extent when the sample nucleates at 53 °C, showing the ability to nucleate in the glassy state, already shown in other polymers. The shape of the DSC thermograms is modeled by using Avrami's theory and allows an estimation of the number of crystallization germs formed. The results of optical microscopy are converted to thermograms by evaluating the average gray level of the image recorded in transmission mode as a function of temperature and calculating its temperature derivative. The shape of such optical thermograms is quite similar to that of the DSC traces but shows some peculiarities after long nucleation treatments. Atomic force microscopy was used to analyze the crystal morphology and is an additional proof of the effect of nucleation in the glassy state. The crystalline morphology observed in samples crystallized after nucleation in the glassy state is qualitatively different from that of samples nucleated above the glass transition temperature, and the number of crystals seems to be much greater than what could be expected from the crystallization kinetics.

Introduction

Poly(L-lactide) is a biocompatible, biodegradable polymer widely used as a biomaterial for several applications including tissue engineering scaffolds.[1−4] In these applications the cell adhesion, growth, and viability have been shown to be strongly affected by characteristics of the surface morphology of the substrate such as roughness. The presence of holes or grooves or microscale texture can induce the cell orientation or cause changes in the cell shape and phenotype (see refs 5−7 and references therein). On the other hand, the kinetics of bioreabsorption "in vivo" is affected by the crystallinity and crystal shape, since the degradation rate of the amorphous domains is faster than that of the crystallites.[8,9] It is therefore interesting to study the possibilities of modifying the crystalline morphology and topography of the semicrystalline surface of the polymer. The size of the spherulites mainly depends on the number of crystals growing simultaneously, i.e., the number of crystal germs. The crystallization rate of PLLA is quite slow; thus, it is possible to get a quasi-amorphous polymer at low temperatures by simply quenching from the melt.[10−14] Even if the crystal growth is nearly null when the glass transition temperature region is reached, the number of crystal nuclei should be considerable, since the nucleation rate increases with the distance to the equilibrium melting temperature. Nucleation progresses with an isothermal annealing at temperatures just above the glass transition temperature. If the temperature is then increased to the interval in which crystal growth is significant, a great number of spherulites grow simultaneously and yield a crystalline morphology very different from that obtained by isothermal crystallization at high temperature after a temperature jump from the melt, or by slow cooling from the melt.[15] In the case of poly(ethylene terephthalate), which also has slow crystallization kinetics, it has been shown that isothermal treatment at temperatures below the glass transition temperature, i.e., the physical aging process, produces ordered domains or physical cross-links that, when the temperature is rapidly increased to a point above the glass transition temperature, in the temperature range in which crystallization takes place, are able to act as crystallization nuclei. The increase in the number of nuclei is detectable by the acceleration of the crystallization kinetics.[16−19] The

* To whom correspondence should be addressed. E-mail: jlgomez@ter.upv.es.

[†] Centro de Investigaciones Científicas del Yucatán.

[‡] Universidad Politécnica de Valencia.

[§] Polymer Engineering Department, University of Minho.

[||] 3B's Research Group—Biomaterials, Biodegradables and Biomimetics, University of Minho.

10.1021/bm050323t CCC: $30.25
Published on Web 09/13/2005

rate of cooling from the melt, even if it is high enough to yield a fully amorphous material, also significantly affects the number of physical cross-links that may act as crystallization nuclei.[20−22]

The aim of this work is to study the formation of crystal nuclei in PLLA by annealing at temperatures just above or just below the glass transition temperature.

Experimental Section

Materials and Methods. PLLA was synthesized by classical polycondensation procedures. The polymerization reactions were carried out as described elsewhere.[23] Briefly, a glass polymerization reactor equipped with a nitrogen flow-through inlet and a vacuum connection was placed in a temperature-controlled bath containing silicone oil. Polymerization was performed in a nitrogen atmosphere at a temperature range of 100−150 °C for 12−48 h. To remove residual monomers, chloroform and methanol were used as solvent and precipitant, respectively. The molecular weights of the polymer, M_n and M_w, were 58000 and 132000, respectively, evaluated by gel permeation chromatography (Shimadzu, LC 10A, Japan) using polystyrene as standard and chloroform as solvent. Samples for DSC experiments of around 4 mg were encapsulated in aluminum pans for solids, which provided good contact between the sample and the bottom and cover of the aluminum pan. Due to the thermal degradation of PLLA at high temperatures, each sample was used for a single DSC scan. Samples for optical microscopy and atomic force microscopy, AFM, were cast from a 1 wt % solution in chloroform on circular microscopy slides. The thickness of the polymer layer was around 5 μm, estimated from the weight of the sample and the PLLA density.

Measurements. DSC experiments were performed in a Pyris 1 apparatus (Perkin-Elmer). Dry nitrogen gas was let through the DSC cell at a flow rate of 20 mL/min. The temperature of the equipment was calibrated by using the melting points of indium and zinc. The heat of fusion of indium was used for calibrating the heat flow. The experiments started with annealing for 2 min at 200 °C, followed by cooling at 40 °C/min to 53 or 73 °C, maintaining this temperature for the desired period, and cooling again to 20 °C. The heating scan followed at 10 °C/min.

Optical microscopy was performed in a Nikon Eclipse E600 microscope, with polarized light, between crossed polarizers. A Linkam THMS600 thermostatic plate refrigerated with a flow of cooling air was used to thermostatize the sample. The temperature calibration was performed with a benzoic acid standard. All the thermal treatments were conducted in the Linkam plate. The sample was initially melted at 200 °C, cooled at the maximum rate allowed by the instrument, to 53 or 73 °C, and maintained at this temperature for the desired time, followed by the heating scan at 10 °C/min. One microphotograph per degree was automatically recorded.

AFM micrographs were recorded with a Nanoscope III from Digital Instruments. The microscope was placed on a vibration-protected table. An SSS-NCH Nanoworld cantilever, with a force constant of 42 N/m and a tip radius with a 5 nm curvature, was used. All the samples were characterized using a set-point amplitude ratio of around 0.7. The thermal treatments were performed on the Linkam plate of the optical microscope. The samples were placed in the AFM device and scanned at ambient conditions.

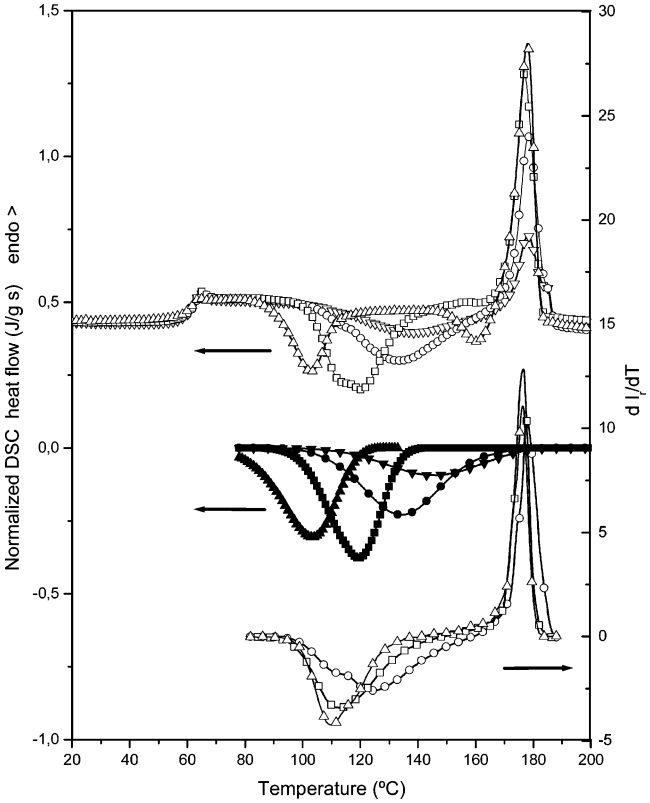

Figure 1. Experimental heating scans performed at 10 °C/min in DSC and optical microscopy after nucleation at 73 °C for 0 (▽), 3 (○), 6 (□), and 12 (△) h. The results of the model simulation of the DSC scans using Avrami's equation are also included (solid symbols).

Results

The DSC heating thermograms show a significant effect of the nucleation treatment on the glass transition and crystallization exotherm. The thermogram recorded immediately after cooling to 20 °C shows the glass transition followed by a broad exotherm between 90 and 160 °C followed by the melting endotherm (Figure 1). The glass transition temperature determined by the midpoint of the rise of the heat capacity in the transition was 61 °C. The isothermal treatment at 73 °C produces a quick shift of the crystallization peak toward lower temperatures (Figure 1). The thermogram recorded after the sample was annealed for 12 h at 73 °C shows two exotherms, one low-temperature exotherm with a minimum at 105 °C, and another at 160 °C, separated by a broad plateau of nearly 30 °C. It was possible to draw a straight line joining the points in the thermogram just after the glass transition and at the highest temperature of the heating ramp. The point at which this baseline crosses the DSC trace corresponds to the point at which the crystal fraction of the sample reaches its maximum value. The area under this line was considered to be the crystallization enthalpy, and is equal to the area on the

Table 1. Crystallization and Melting Enthalpy Calculated in the Heating Scans after Different Nucleation Treatments[a]

nucleation annealing	Δh_{cryst} (J/g)	Δh_{melt} (J/g)	$x_{cryst,max}$ (%)	$x_{cryst,max}$ (%) (model)
no isothermal annealing	−15.3	16.0	16	21
73 °C for 3 h	−32.0	34.0	34	33
73 °C for 6 h	−38.2	38.8	41	40
73 °C for 12 h	−28.7, −6.5	40	31, 7	43
53 °C for 3 h	−17.5	17.6	19	22
53 °C for 6 h	−22.6	22.6	24	27
53 °C for 12 h	−33.5	33.2	36	32

[a] The experimental maximum crystallinity reached in the scan, $x_{cryst,max}$, and the values calculated for $x_{cryst,max}$ using Avrami's model are also listed.

baseline corresponding to the melting peak, as can be expected due to the fact that the crystallinity at the beginning of the thermogram is nearly null. This behavior was also found in the thermograms recorded after the different thermal treatments, with the exception of the thermogram recorded after annealing for 12 h at 73 °C. In this case, the total area of the two exotherms is only 35.2 J/g but the melting enthalpy is 40 J/g, which means that some crystal growth takes place at 73 °C. The area of the exotherm after cooling from the melt without isothermal annealing was only 15.3 J/g, which means, assuming a value of 93 J/g for the melting enthalpy of the single crystal,[24] that the crystal fraction being built up during the heating scan is 16%. The crystallization enthalpy increases with the nucleation treatment at 73 °C for 3 and 6 h (Table 1); the crystal fraction increases to 34% and 41%, respectively. The maximum crystal fraction in the sample annealed for 12 h at 73 °C would be 43%, determined from the melting peak. The difference between the melting enthalpy and the sum of the two crystallization exotherms is 4.8 J/g, which means that at the beginning of the DSC scan, i.e., at the end of the isothermal period, the crystallinity would be 5%.

The scans recorded after annealing at 53 °C show the endotherm overshoot in the glass transition due to physical aging, followed by the cold crystallization exotherm, whose temperature is always higher than after annealing at 73 °C (Figure 2). Nevertheless, the crystallization enthalpy after 12 h reaches 33.5 J/g, which means that the maximum degree of crystallinity attained during the heating scan reaches 36%, not far from the values found after annealing above the glass transition temperature (Table 1).

Isothermal crystallization experiments were conducted at 120 °C after the different nucleation annealings. The DSC traces (Figure 3) show that the kinetics of crystallization becomes faster with longer annealing times, at both 53 and 73 °C. After 12 h at 73 °C the peak appears before the stabilization of the temperature after the jump from 73 to 120 °C.

The results of optical microscopy are shown in Figures 1 and 2 as plots of the derivative of the average gray level of the image recorded in transmission mode as a function of temperature during the heating scan. It is interesting to note that these thermograms are quite similar to those obtained by DSC but show some peculiarities, mainly in the case of the heating scan conducted after annealing for 12 h at 73 °C. In optical microscopy the high-temperature crystallization peak that shows the DSC trace does not appear.

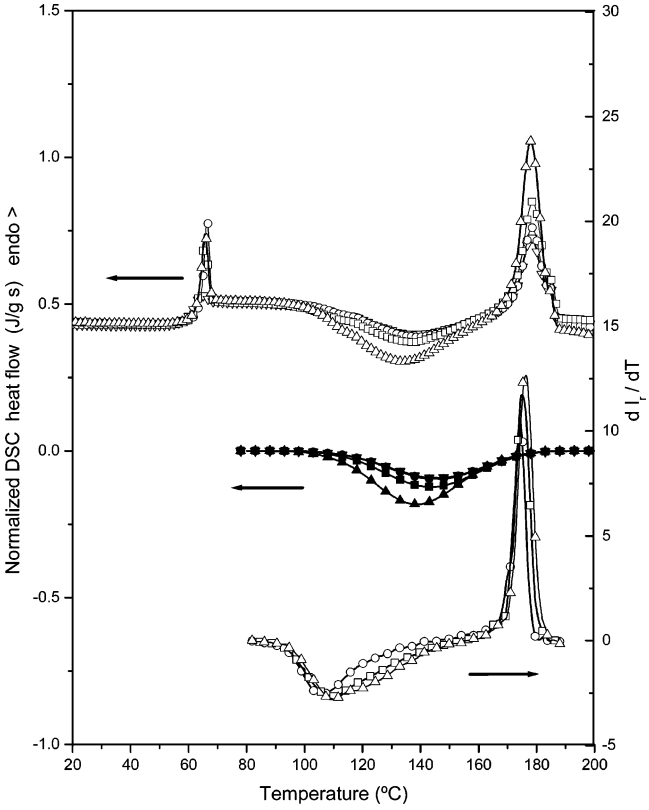

Figure 2. Experimental heating scans performed at 10 °C/min in DSC and optical microscopy after nucleation at 53 °C for 0 (▽), 3 (○), 6 (□), and 12 (△) h. The results of the model simulation of the DSC scans using Avrami's equation are also included (solid symbols).

The change in the crystal morphology was studied by atomic force microscopy. Figure 4 shows the topography pictures corresponding to samples crystallized at 120 °C after different thermal treatments. The isothermal crystallization for 2 h at 120 °C after a temperature jump from the melt shows large spherulites. The roughness of the surface can be seen from the depth of the color scale generated in Figure 4a. The height difference between the black and bright-yellow zones is about 1 μm. To emphasize this feature, the cross-section along the straight line shown in Figure 4a has been drawn in Figure 6.

Figure 4b shows the topography of the sample crystallized for 2 h at 120 °C after the sample was cooled to 73 °C and immediately reheated to 120 °C. The spherulites are much smaller than those shown in Figure 4a. The effect of nucleation at 73 °C is shown in Figure 4c. After 6 h the decrease in the size of the spherulites demonstrates the increase in the number of crystallization nuclei at the start of the isothermal crystallization at 120 °C.

Figure 4d shows the effect of cooling the sample to 53 °C, producing the vitrification of the sample, and immediately increasing the temperature to 120 °C. The differences with the results of cooling to 73 °C (Figure 4b) are not significant. In fact, pictures taken of different samples subjected to identical thermal treatments can differ from one another in the same order as Figure 4b,d. The effect of nucleation at 53 °C is shown in Figure 4e and corresponds to the nucleation for 6 h. The picture shown corresponds to a surface of 50 × 50 μm (as in Figure 4a−d). The cross-section along the line shown in Figure 4e is shown in Figure

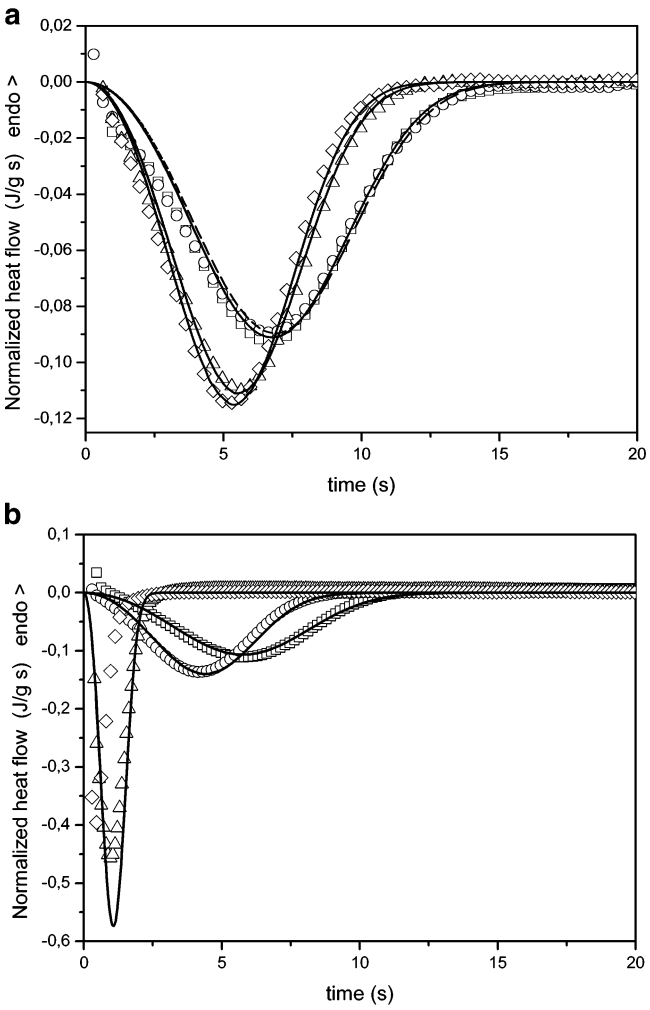

Figure 3. DSC heat flow measured during the isothermal crystallization at 120 °C after nucleation at 53 °C (a) and 73 °C (b) for 0 (□), 3 (□), 6 (△), and 12 (◇) h. The solid lines correspond to Avrami's equation with exponent 3.

6. This topography is characteristic of the structure in which the growth of the spherulites is not complete. To show this more clearly, Figure 5a presents the topography of the sample nucleated for 6 h at 53 °C recorded in a scan of a 5 × 5 μm surface. For comparison, a scan with the same magnification was recorded of a sample nucleated for 6 h at 73 °C.

Discussion

The analysis of the crystallization kinetics can be made on the basis of Avrami's general theory,[24] which for the isothermal crystallization yields the well-known equation

$$1 - \frac{v_c}{v_\infty} = \exp(-K(T)t^n) \qquad (1)$$

where v_c is the volume crystal fraction, $v_{c,\infty}$ is its maximum value at infinite time, t is time, and n is Avrami's exponent that depends on the nucleation and growth mechanisms.

In the case of the crystallization after different nucleation annealings, one may assume that, after cooling to a temperature in the range of the glass transition temperature, the number of nuclei formed in the amorphous material is high enough to consider that the crystallization that takes place

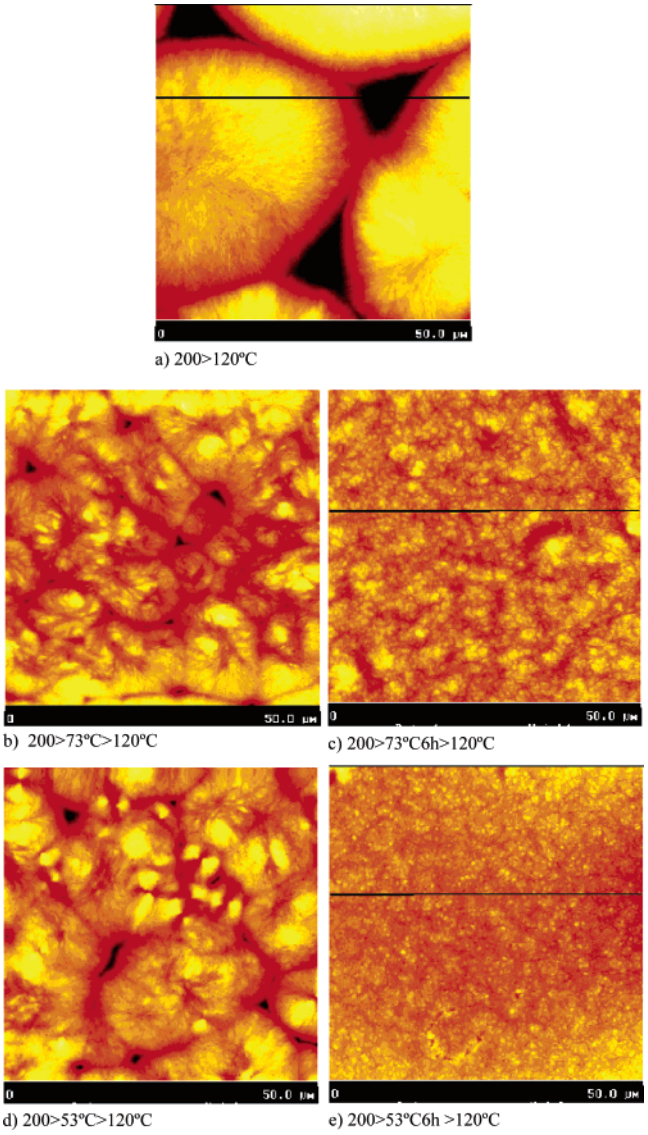

Figure 4. AFM pictures of the topography of samples crystallized for 2 h at 120 °C after different nucleation treatments (the picture dimensions are 50 × 50 μm): (a) temperature jump from 200 to 120 °C, (b) sample suddenly cooled from 200 to 73 °C and immediately reheated to 120 °C prior to crystallization, (c) sample nucleated for 6 h at 73 °C, (d) sample suddenly cooled from 200 to 53 °C and immediately reheated to 120 °C prior to crystallization, (e) sample nucleated for 6 h at 53 °C.

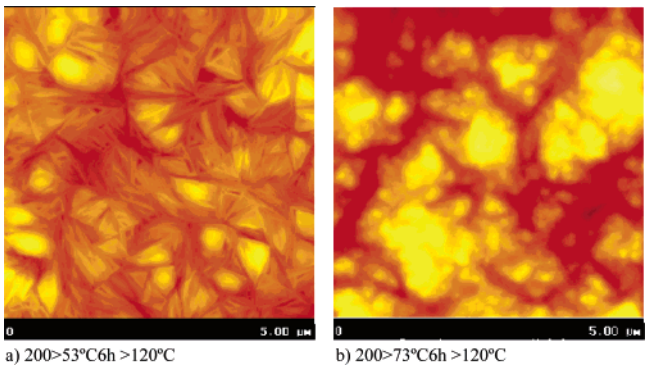

Figure 5. AFM topography in a 5 × 5 μm surface of samples nucleated with the same thermal treatments as in parts e and c of Figure 4, respectively.

afterward at higher temperatures, cold crystallization, is athermal; i.e., the number of nuclei formed during the

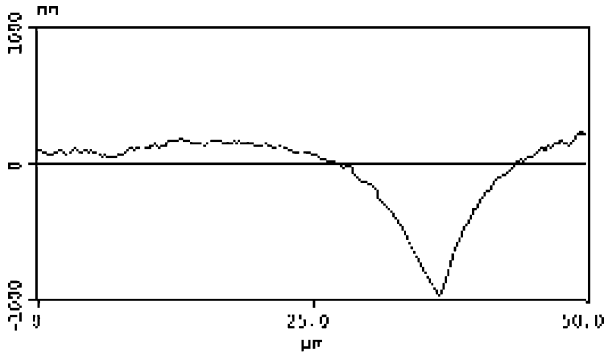

a) Cross-section of Figure 4a

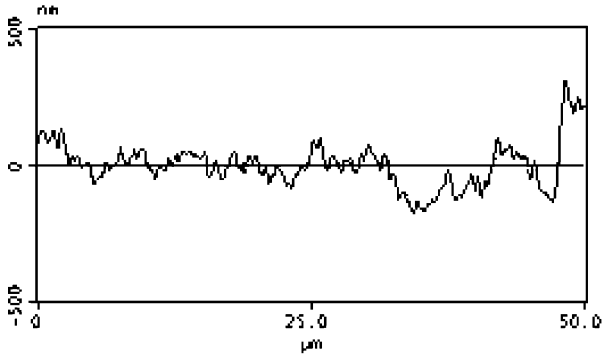

b) Cross-section of Figure 4c

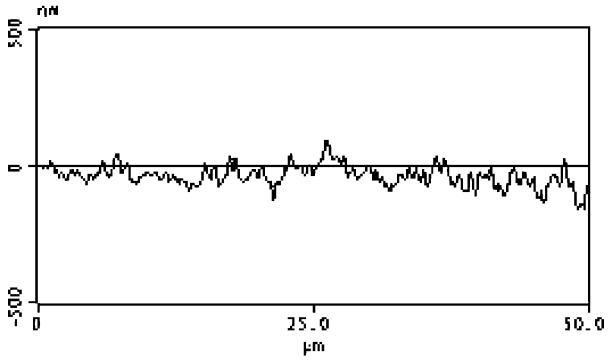

c) Cross-section of Figure 4e

Figure 6. Cross-section of the pictures shown in parts a, c, and e of Figure 4, (a), (b), and (c), respectively, along the straight lines shown in the figures.

crystallization is small compared with that of nuclei existing at the beginning of the process. In this situation, Avrami's theory (considering isothermal spherical crystal growth) yields

$$1 - \frac{v_c}{v_\infty} = \exp\left(-\frac{4}{3}\pi G^3 z t^3\right) = \exp(-K(T)t^3) \qquad (2)$$

where G is the radial crystal growth rate and z is the number of nuclei per unit volume. Avrami's exponent 3 is characteristic of the athermal crystallization with spherical growth. A growth mechanism with Avrami's coefficient 3 was found to accurately describe cold crystallization of PET.[21] The fit of eq 2 to the results shown in Figure 3 allows the kinetic constant K at 120 °C to be calculated. The fits were performed considering v_∞ (the same for all the nucleation treatments) and K (which depends on the number of nuclei and thus on the temperature and duration of the annealing) as fitting parameters. A value of 93 J/g was assumed for the melting enthalpy, and a value of 1.29 g/cm^3 was taken for the density of the crystalline phase.[26] The results of the fits are shown in Table 2. The constant K is proportional to the number of nuclei z, according to eq 2. The increase in the number of nuclei accelerates the crystallization process. On the other hand, the crystal growth rate G may be considered a function of temperature, independent of z. Thus, the ratio $z(T_n,t_n)/z(T_n,0)$, the ratio of the number of nuclei after nucleation at temperature T_n for a time t_n to the number of nuclei after cooling to T_n and an immediate jump to the crystallization temperature, can be obtained from the values obtained for K. The study of the crystallization kinetics using Avrami's equation can thus be used to characterize the number of effective nuclei. A similar method was proposed in ref 19 to evaluate the efficiency of nucleating additives in isotactic polypropylene. The results listed in Table 2 show that the acceleration observed in the isothermal crystallization at 120 °C after nucleation at 53 °C can be explained if the number of effective nuclei formed by annealing the sample at 53 °C for 12 h is twice the number formed during cooling to 53 °C. This ratio increases to 160 in the case of the annealing for 6 h at 73 °C. In the case of the 12 h treatment at this temperature, the crystallization exotherm takes place for periods too short to attempt an evaluation.

The acceleration of the crystallization is also clear in the heating scans after nucleation treatments. The cold crystallization peak shifts toward lower times with increasing nucleation times at both 53 and 73 °C. An evaluation of these experimental results can also be achieved using Avrami's theory. To achieve this, the heating ramp was simulated with a series of 1 deg temperature steps followed by isothermal stages with a duration such that the average increase of temperature was the experimental one. The crystal fraction at the beginning of the isothermal step at temperature T_i was considered equal to the crystallinity at the end of the previous step at T_{i-1}, which will be called $v_{c,i-1}$. At this moment a fictive time $t_{fic,i}$ was defined as the time at which the crystal fraction $v_{c,i-1}$ would be reached in an isothermal crystallization at temperature T_i starting with the fully amorphous material

$$t_{fic,i} = \left\{-\frac{1}{K(T_i)}\ln\left(1 - \frac{v_{c,i-1}}{v_\infty}\right)\right\}^{1/n} \qquad (3)$$

and the crystal fraction at the end of the isothermal stage at temperature T_i results in

$$v_{c,i} = v_\infty[1 - \exp(-K(T)(t_{fic,i} + 1/\beta)^n)] \qquad (4)$$

where β is the heating rate. The derivative of the simulated $v_c(T)$ curve was then used to calculate the heat flow:

$$\dot{q}(T) = \beta\rho\Delta h^{sl}\frac{dv_c}{dT} \qquad (5)$$

where Δh^{sl} is the melting enthalpy and ρ is the density of the crystal phase.

The simulation requires information on the temperature dependence of K, which according to eq 2, for a given nucleation treatment, is proportional to the crystal growth

Table 2. Parameter K of Avrami's Equation Determined at 120 °C from Fitting to Eq 2 of Isothermal Crystallization Experiments and from Fitting to Eq 7 of Heating Scans after Different Nucleation Treatment and the Ratios of the Number of Nuclei after Nucleation Relative to the Sample Cooled to the Annealing Temperature and Immediately Reheated to 120 °C (See the Text)

nucleation annealing	K(120 °C) (s^{-3}) from isothermal crystallization	$z(T_n,t_n)/z(T_n,0)$	$A_j(T_n,t_n)/A_j(T_n,0)$	K(120 °C) (s^{-3}) from heating scans
200 °C > 120 °C	1.5×10^{-9}			
200 °C > 73 °C >120 °C	1.6×10^{-8}	1	1	1.1×10^{-8}
200 °C > 73 °C (3 h) > 120 °C	3.6×10^{-8}	2.3	5	5.0×10^{-8}
200 °C > 73 °C (6 h) > 120 °C	2.5×10^{-6}	160	30	3.0×10^{-7}
200 °C > 73 °C (12 h) > 120 °C			40	4.0×10^{-7}
200 °C > 53 °C > 120 °C	9.5×10^{-9}	1	1	1.0×10^{-8}
200 °C > 53 °C (3 h) > 120 °C	1.0×10^{-8}	1.05	1.05	1.1×10^{-8}
200 °C > 53 °C (6 h) > 120 °C	1.8×10^{-8}	1.9	1.5	1.5×10^{-8}
200 °C > 53 °C (12 h) > 120 °C	2.0×10^{-8}	2.1	5	3.1×10^{-8}

rate $G(T)$, and can be considered independent of the number of nuclei. M. L. DiLorenzo[12] found a temperature dependence of the spherulite growth in PLLA according to the theory of Lauritzen and Hoffman:[27,28]

$$G = G_0 \exp\left(\frac{-U}{R(T_c - T_\infty)}\right) \exp\left(\frac{-K_g}{T_c(T_m - T_c)}\right) \qquad (6)$$

According to the theory of Lauritzen and Hoffman, the value of K_g depends on the crystal growth regime. In PLLA a transition from regime II (T > 115 °C) to regime III (T < 115 °C) was found in which K_g duplicates according to the theory.[12,13,29]

To introduce this information into the simulation, a function $K_j(T)$ has been used for each nucleation treatment j, according to the equation

$$K_j(T) = A_j(T_n,t_n) \exp\left(\frac{-B}{(T_c - T_\infty)}\right) \exp\left(\frac{-C}{T_c(T_m - T_c)}\right) \qquad (7)$$

with $T_\infty = 308$ K[13] and $T_m = 480$ K.[30] The functions $K_j(T)$ only depend on the nucleation treatment through a multiplicative constant $A(T_n,t_n)$ that is proportional to the number of nuclei, z_j. In the value of the constants $A(T_n,t_n)$ and C the transition from regime II to regime III mentioned above was considered. The value of C in eq 7 above 115 °C was considered to be twice the value assumed for lower temperatures in the heating scan. The value of $A(T_n,t_n)$ changes correspondingly to keep the continuity of $K_j(T)$ at 115 °C. A value of the limit crystal fraction $\upsilon_{c,\infty} = 0.4$ was assumed, according to the experimental results.

The parameters $A(T_n,t_n)$, B, and C were obtained by least-squares fitting of the model simulation to the experimental thermograms. The results of the simulation are shown in Figures 1 and 2. The ratios $A(T_n,t_n)/A(T_n,0)$ are listed in Table 2, and the other parameters were $B = 832$ K and $C = 513000$ K^2 in regime III, at low temperatures. Table 2 shows the values of $K_j(T)$ at 120 °C as obtained with the fitting of the experimental heating scans to eq 7. The results sensibly agree with the values determined from the fitting to eq 2 of the isothermal crystallization kinetics at this temperature. According to these values, the maximum value of $K(T)$ and thus the maximum crystal growth rate take place at 130 °C, which closely corresponds to the results of ref 12. This feature was confirmed in the sample used in this work following the spherulite growth in optical microscopy. The samples were suddenly cooled to three different temperatures (140, 131, and 123 °C) from the melt, and the spherulite diameter was measured as a function of time. The values of the growth rates $G(140\ °C) = 0.024\ \mu$/s, $G(131\ °C) = 0.059\ \mu$/s, and $G(123\ °C) = 0.046$ m/s confirm the results of the fits to the DSC cold crystallization peaks with respect to the temperature of the maximum crystal growth. The simulation correctly reproduces the cold crystallization exotherm after nucleation at 53 °C. The fact that the maximum crystalline fraction attained in the heating scan increases with the annealing time at 53 °C (Table 2) is also correctly reproduced. On the other hand, the ratios between the number of nuclei formed for the different annealing times agree with the results of the isothermal crystallization experiments.

In the case of the nucleation treatments at 73 °C, the simulation correctly predicts the scans measured after 3 or 6 h of annealing, but in the latter case the ratio $A(73,6)/A(73,0)$ is much smaller than the ratio obtained from the isothermal experiments. Something similar would happen in the case of nucleation for 12 h at 73 °C. Although in this case it was impossible to determine the nuclei ratio from the isothermal experiments, it obviously must be much higher than in the scans. This could imply that during the scans part of the nuclei are dissolved between glass transition and the beginning of crystal growth, a behavior very different from what happens in the case of the nuclei formed at 53 °C. The increase in the maximum crystallinity reached during the scan with the number of nuclei is also correctly reproduced for nucleation times of 3 and 6 h. The scan after 12 h at 73 °C shows a cold crystallization peak more or less of the same height as after 6 h. This feature could only be reproduced in the simulation when a 5% initial crystallinity was considered, according to the results shown in Table 1 (the curve shown in Figure 1 for the computer simulation was obtained under this assumption). Obviously, only the low-temperature exotherm was simulated.

It can therefore be concluded that the crystallization kinetics are well described with Avrami's theory using Avrami's exponent $n = 3$. The differences in the nucleation kinetics can be explained by the difference in the number of nuclei formed as a result of the annealing at low temperature. In the case of the annealing at 53 °C, the crystal nuclei would be formed due to the contraction of the material during

physical aging that would form ordered structures that act at higher temperatures as crystallization germs. It is worth noting that in amorphous materials after physical aging, when the sample temperature increases to a value just above the glass transition temperature, the macroscopic thermodynamic variables revert to their equilibrium values, regardless of the previous thermal history. Nevertheless, in the case of amorphous PET, the reversibility of the enthalpy in samples subjected to aging below T_g and kept for a short time at a temperature above T_g was not complete.[20] The crystallization studies show that at least part of the ordered structures formed in PLLA during physical aging persist above the glass transition temperature. This occurs not only in the case of a sudden jump in temperature to 120 °C but also in a heating scan with a considerable lapse of time between the moment when the sample devitrifies and the start of the crystallization process.

This feature is further confirmed by optical microscopy experiments. In the heating scans the peaks of the derivative of the transmitted light are steeper than the exotherms in the DSC scans. A similar feature was found in ref 16 when the shapes of the crystallization profile followed by optical microscopy, infrared analysis, and X-ray scattering in isothermal processes were compared. It seems that the growth of the crystallites is detected at the first stages of the crystallization process, and on the other hand, part of the crystal formation that takes place with high crystal fractions is not able to increase the birrefringence of the material and thus does not contribute to the intensity of the light transmitted through the sample. This seems in particular to be the case of the high-temperature crystallization endotherm shown in DSC after nucleation for 12 h at 73 °C. This leaves no trace in the optical microscopy thermogram. But the effect of the nucleation treatment is quite clear in the optical microscopy results shown in Figures 1 and 2. This is an additional proof of the fact that the ordered structures formed below T_g are not dissolved during the heating scan between the glass transition and the start of the crystallization.

The AFM results are nevertheless surprising and seem to contradict the analysis of the DSC results explained above. Clearly, the number of crystals observed in the sample nucleated at 53 °C for 6 h (Figure 4e) is much larger than in the samples cooled to 53 or 73 °C and immediately reheated to 120 °C, even larger than in the sample nucleated at 73 °C for 6 h. The crystallization kinetics after nucleation at 73 °C is much faster than after nucleation at 53 °C. This supports the fact that the number of effective nuclei in the crystallization is larger in the former case. The calculations based on Avrami's model support this conclusion. It seems that the role played by the nuclei formed below the glass transition temperature in the crystallization process is quite different from that of the nuclei formed above T_g. The observation of the sample surface at a higher magnification shows a different structure of the crystals after nucleation for 6 h at 53 or 73 °C (the topography of the samples nucleated in annealings of 12 h are nearly identical to those shown for 6 h annealings).

The structure of the ordered regions formed during physical aging in the glassy state is still unclear. The conformational mobility in the glassy state produces a densification of the material, but the ability to create ordered, paracrystalline, structures should be very restricted. The situation is very different from the result of the annealing at temperatures just above T_g, where, as shown by the DSC results, even a small crystal fraction can be formed for long annealing times. It seems acceptable that the molecular organization in the nuclei formed below T_g must be quite different from that of the nuclei formed above T_g. Nevertheless, it can be concluded that the formation of these ordered regions in the glassy state is not reversible when the material devitrifies with an increase in temperature. The number of such ordered regions that are effective as crystallization nuclei as deduced from the number of crystallites observed in AFM is quite large; nevertheless, the crystallization kinetics is too slow for that number of nuclei according to Avrami's formalism. On the other hand, the qualitative comparison of the topography of the samples nucleated for 6 h at 73 °C and those cooled to 73 °C and immediately reheated to the crystallization temperature seems to correspond to the ratios of nuclei determined from the DSC isothermal experiments.

New experiments and the use of different techniques are necessary to characterize the structure of the nuclei formed in the glassy state of polymers that are able to crystallize. A more detailed study of the surface of semicrystalline samples using AFM, exploiting the measurement of the phase angle at high magnification to characterize the size and shape of the crystal lamellae, could be expected to be useful in this study. These experiments are currently in progress.

Conclusions

Isothermal annealing of amorphous PLLA at temperatures below the glass transition temperature forms ordered structures that on further heating above T_g are able to act as crystallization nuclei, as confirmed by DSC and optical microscopy experiments. Avrami's theory can be applied to analyze the crystallization kinetics of PLLA, both isothermal and during heating scans. The acceleration of the crystallization process after nucleation treatments can be explained by the increase in the number of the nuclei at the beginning of crystallization in the case of nucleation above the glass transition temperature. Nevertheless, the number of crystallites observed by AFM after nucleation in the glassy state seems incompatible with the slow crystallization kinetics observed by DSC. The structure of the crystallites also seems to be different after nucleation below or above the glass transition temperature.

Acknowledgment. We are grateful to Kadriye Tuzlakoglu for providing the PLLA used in this work. M.S.S. and J.L.G.R. acknowledge the support of CICYT through Project MAT2004-04980-C02-01 and the support of their research group by the Generalitat Valenciana through Project GRUPOS03/018. J.L.G.R. expresses his gratitude to the Universidad Politécnica de Valencia (UPV) for funding his stay at the Centro de Investigaciones Científicas del Yucatán, Mérida, Mexico. AFM was conducted by the Microscopy

Service of the UPV, whose advice was greatly appreciated. We thank the R+D+i Linguistic Assistance Office at the UPV for their help in revising this paper.

References and Notes

(1) Södegard, A.; Stolt, M. *Prog. Polym. Sci.* **2002**, *27*, 1123.
(2) Thomson, R. C.; Wake, M. C.; Yaszemski, M. J.; Mikos, A. G. *Adv. Polym. Sci.* **1995**, *122*, 245.
(3) Kim, H. D.; Bae, E. H.; Kwon, I. C.; Pal, R. R.; Nam, J. D.; Lee, D. S. *Biomaterials* **2004**, *25*, 2319.
(4) Ma, Z.; Gao, C.; Gong, Y.; Shen, J. *Biomaterials* **2005**, *26*, 1253.
(5) Saltzman, W. M. In *Principles of Tissue Engineering*, 2nd ed.; Lanza, R. P., Langer, R., Vacanti, J., Eds.; Academic Press: San Diego, 2000; Chapter 19.
(6) Patrick, C. W., Mikos, A. G., McIntire, L. V., Eds. *Frontiers in Tissue Engineering*; Pergamon: New York, 1998.
(7) Lee, S. J.; Choi, J. S.; Park, K. S.; Khang, G.; Lee, Y. M.; Lee, H. B. *Biomaterials* **2004**, *25*, 4699.
(8) Reeve, M.; McCarthy, S.; Downey, M.; Gross, R. *Macromolecules* **1994**, *27*, 825.
(9) MacDonald, R.; McCarthy, S.; Gross, R. *Macromolecules* **1996**, *29*, 7356.
(10) Iannace, S.; Nicolais, L. *J Appl. Polym. Sci.* **1997**, *64*, 911.
(11) Miyata, T.; Masuko T. *Polymer* **1998**, *39*, 5515.
(12) Di Lorenzo, M. L. *Polymer* **2001**, *42*, 9441.
(13) Salmerón Sánchez, M.; Gómez Ribelles, J. L.; Hernández Sánchez, F.; Mano, J. F. *Thermochim. Acta* **2005**, *430*, 201.
(14) Wang, Y.; Gómez Ribelles, J. L.; Salmerón Sánchez, M.; Mano, J. F. *Macromolecules* **2005**, *38*, 4712.
(15) Pluta, M.; Galeski, A. *J. Appl. Polym. Sci.* **2002**, *86*, 1386−1395.
(16) Bove, L.; D'Aniello, C.; Gorrasi, G.; Guadagno, L.; Vittoria, V. *Polym. Bull.* **1997**, *38*, 579.
(17) McGonigle, E. A.; Daly, J. H.; Gallager, S.; Jenkins, S. D.; Liggat, J. J.; Olsson, I.; Pethrick, R. A. *Polymer* **1999**, *40*, 4977.
(18) Santa Cruz, C.; Baltá Calleja, F. J.; Zachmann, H. G.; Stribeck, N.; Asano, T. *J. Polym. Sci., Part B: Polym. Phys.* **1991**, *29*, 819.
(19) Fillon, B.; Lotz, B.; Thierry, A.; Wittmann, J. C. *J. Polym. Sci., Part B: Polym. Phys.* **1993**, *31*, 1395.
(20) Kiflie, Z.; Piccarolo, S.; Vassileva, E. *Macromol. Symp.* **2002**, *185*, 35.
(21) Kiflie, Z.; Piccarolo, S.; Brucato, V.; Baltá-Calleja, F. J. *Polymer* **2002**, *43*, 4487−4493.
(22) Baltá-Calleja, F. J.; García Gutiérrez, M. C.; Rueda, D. R.; Piccarolo, S. *Polymer* **2000**, *41*, 4143.
(23) Yavuz, H.; Babac, C.; Tuzlakoglu, K.; Piskin, E. *Polym. Degrad. Stab.* **2002**, *75*, 431.
(24) Fisher, E. W.; Sterzel, H. J.; Wegner, G. *Kolloid Z. Z. Polym.* **1973**, *251*, 980.
(25) Avrami, M. *J. Chem. Phys.* **1940**, *8*, 212.
(26) Brandrup, J., Immergut, E. H., Grulke, E. A., Eds. *Polymer Handbook*; Wiley-Interscience: New York, 1999.
(27) Hoffman, J. D.; Davis, G. T.; Lauritzen, J. I. *Treatise on solid-state chemistry: crystalline and non-crystalline solids*; Plenum Press: New York, 1976.
(28) Hoffman, J. D. *Polymer* **1983**, *24*, 3.
(29) Iannace, S.; Maffezzoli, A.; Leo, G.; Nicolais, J. *Polymer* **2001**, *42*, 3799.
(30) Vasanthakurami, R.; Pennings, A. J. *Polymer* **1983**, *24*, 175.

BM050323T